4

Manipulation of Photonic Orbital Angular Momentum for Quantum Information Processing

Eleonora Nagali and Fabio Sciarrino
Dipartimento di Fisica, Sapienza Universitá di Roma
Italy

1. Introduction

More than a century ago, pioneering works carried out by Poynting (1909) and other physicists have provided the evidence of the validity of Marxwell equations for an electromagnetic field, showing how a beam of light carries energy and momentum, both in the linear and angular components. In particular the angular momentum of light, related to the generator of rotations in quantum mechanics, has been typically associated with its polarization, and more specifically with its circular polarization components. An optical beam traveling in the positive direction of the z axis that is circularly polarized, carries a z-component angular momentum content $\sigma = \pm\hbar$ per photon, which is positive if the circular polarization is left-handed and negative if it is right-handed. This angular momentum content is not just a formal property, but a very concrete one that can have significant mechanical effects as for example an observable induced rotation by absorption to a material particle Beth (1936); Friese et al. (1998)

At the same time, calculations of angular momentum for a free electromagnetic beam gave rise to a *second* contribution not related to photon spin, to which was attributed the name of *orbital angular momentum* (OAM). Unlike the spinorial angular momentum (SAM), considered as the intrinsic part of angular momentum since it does not depend on the specific reference frame, the orbital component is associated to the transverse spatial structure of the wavefront. More precisely, this angular momentum appears when the beam wavefront acquires a helicoidal structure, or equivalently, its field spatial dependence contains a helical phase factor having the form $e^{im\varphi}$, where φ is the azimuthal phase of the position vector r around the beam axis z and m is any integer, positive or negative, providing the direction and the "velocity" of the phase spiraling along the beam direction. It can be shown that in this case the optical beam carries an angular momentum along its axis z equal to $m\hbar$ per photon, in addition to the polarization one σ. When m is nonzero, the helical phase factor imposes the existence of an optical vortex at the center of the beam where the light intensity vanishes. Although the fundamental concept of orbital angular momentum associated with a light field was already known since the early forties, the research on the orbital angular momentum of light has begun only in 1992, with the appearance of a seminal publication carried out by Allen et al. (1992). In this work, Allen et al. demonstrated experimentally that a particular set of solutions of Helmoltz equation in paraxial approximation, the Laguerre-Gauss modes (LG), carry a fixed amount of orbital angular momentum. Moreover, such beam could be

generated experimentally in the laboratory by manipulating gaussian beams emerging from a laser cavity. Interestingly, even though it was largely diffused to indicate the "single-photon contribution" to the whole value of OAM carried by the beam, the first experimental test on the OAM as an individual property of single photons has been carried out only in 2001 by Mair et al. (2001)

For all the reasons listed above, the orbital angular momentum is considered a recently discovered photonic degree of freedom. In general, only the global angular momentum is associated to an observable quantity, however in the paraxial approximation, both SAM and OAM can be manipulated and measured separately. Indeed the OAM of light can be exchanged with matter, thus opening new perspectives in several fields of classical and quantum physics as well as in biology. In contrast to SAM, which couples only with the material local anisotropy (birefringence), OAM couples mainly with material inhomogeneities characterized by a rotational asymmetry around the beam axis. This coupling may be considered a negative feature when OAM is considered for communication purposes, as it makes it very sensitive to turbulence or other sources of noise Paterson (2005), but it becomes an useful property when OAM is adopted as a tool for sensitively probing the properties of a given medium as considered in several recent works (see Molina-Terriza, Rebane, Torres, Torner & Carrasco (2007); Torner et al. (2005)). The use of OAM for probing can lead to microscopic imaging with a spatial resolution that is higher than the Rayleigh limit Tamburini et al. (2006) and, when OAM fields are used in combination with suitable fluorescence methods (e.g., the stimulated emission depletion), they enable new methods of far-field microscopy with theoretically unlimited resolution Harke et al. (2006); Hell (2009). Optimal spatially structured light beams have also been considered as tools to cage/uncage specific molecules for accurate and rapid biological imaging Shoham et al. (2005). Some of these approaches may have relevant applications in the imaging of biological tissues, e.g. for diagnostic or research purposes. Finally the characteristic doughnut profile of the intensity pattern of a LG mode allows an efficient ion and atom trapping with low scattering and hence heating of the atom, useful for atom optics and BECs purposes Andersen et al. (2006).

Beyond all these applications, it has been recognized that the orbital angular momentum has a great potential for quantum photonics, in particular regarding quantum information protocols implemented through quantum optics techniques. Quantum information (QI) is based on the combination of classical information theory and quantum mechanics. In the last few decades, the development of this new field has opened far-reaching prospects both for fundamental physics, such as the capability of a full coherent control of quantum systems, as well as in technological applications, most significantly in the communication field. In particular, quantum optics has enabled the implementation of a variety of quantum information protocols. The fundamental unit of information in QI theory is a two-level system, the quantum bit or qubit. Exploiting the features of quantum states, however, it has been proven that qubits allows the transfer of more information than the one encoded in a classical boolean alphabet and, at the same time, the quantumness of qubit systems ensure high level of security in communication processing. In this context, the information encoding based on two-dimensional system can be experimentally implemented by exploiting degrees of freedom of single photons as, for example, the polarization. Up to now, several quantum information protocols have been successfully implemented, thanks to a notable control on the polarization degree of freedom achieved through different efficient devices. However

there may be a significant advantage in introducing the use of higher dimensional systems for encoding and manipulating the quantum information. Such *d*-level quantum systems, or *qudits*, provide a natural extension of qubits that has been shown to be suitable for prospective applications such as quantum cryptography and computation Cerf et al. (2002); Lanyon et al. (2009). In this framework the orbital angular momentum, defined in an infinitely dimensional Hilbert space, provides a natural choice for implementing *qudits* encoded in a single photon state (see Franke-Arnold et al. (2008); Molina-Terriza, Torres & Torner (2007)). This can be an important practical advantage, as it allows increasing the information content per photon, and this, in turn, may cut down substantially the noise and losses arising from the imperfect generation and detection efficiency, by reducing the total number of photons needed in a given process. Moreover, the combined use of different degrees of freedom of a photon, such as OAM and spin, enables the implementation of entirely new quantum tasks, as shown by Aolita & Walborn (2007); Barreiro et al. (2005; 2008)

Since the seminal paper of 1992 a large effort has been spent to develop optical tools able to manipulate and control efficaciously the orbital angular momentum degree of freedom. Up to now, by observing the transfer of OAM to matter, some devices have been adopted in order to generate/analyse LG modes (computer generated holograms, spatial light modulators), or manipulate the OAM analogously to what is commonly carried out through waveplates on polarization (cylindrical lenses mode converters). Despite these successes, the optical tools for controlling the OAM quantum states remain rather of limited use: a wider and more practical control of the OAM resource somehow analogous to that currently possible for the polarization degree of freedom is by the way under progress.

Here we present a brief introduction on orbital angular momentum in quantum optics, describing the main devices adopted in order to achieve an efficient manipulation. Furthermore, we describe some experiments that have been carried out by adopting an optical device, the *q-plate*, able to couple the spinorial and orbital contributions of the angular momentum of light by exploiting the properties of liquid crystals.

2. The orbital angular momentum of light

Light beams carry energy and momentum, the latter both in its linear and angular components. Thus, when an electromagnetic field interacts with matter, an exchange of energy and momentum occurs, manifested in interesting mechanical effects or in changing of the beam properties. Here we will focus on light angular momentum, composed by a spinorial and orbital component. The manipulation of spinorial angular momentum (SAM), commonly associated to the polarization of light, is largely diffused in all the different field of physics. On the other hand, the orbital angular momentum (OAM) of light did not go through the same diffusion for many years, since after seminal works of Poynting (1909) and Beth (1936), only in 1992 Allen et al. (1992) demonstrated that particular solutions of the Helmoltz equation in the paraxial regime exhibit an azimuthal phase structure typical of beams possessing OAM. Such beams, as for example the Laguerre-Gauss beams, can be experimentally manipulated and thus offer a valuable resource in quantum information, where the possibility to exploit the infinite-dimensionality of OAM opens interesting perspectives. Here we present theoretically the main elements that characterize, both in classical and quantum regimes, the orbital angular

momentum of light, deriving the solutions of Helmoltz equation and presenting the main ones, namely the Hermite-Gauss and Laguerre-Gauss beams.

3. Classical orbital angular momentum of light

In classical physics the total angular momentum $\vec{J}$ of an electromagnetic field reads:

$$\vec{J} = \epsilon_0 \int d\vec{r}\vec{r} \times (\vec{E} \times \vec{B})$$

where $\vec{E}$ and $\vec{B}$ are the electric and magnetic fields, respectively. The angular momentum is a conserved quantity for a free field, due to the invariance under arbitrary rotations of free Marxwell equations Enk & Nienhuis (1994). Moreover, as the electric field can be separated in longitudinal and transverse component $\vec{E} = \vec{E}_{||} + \vec{E}_{\perp}$, it is possible to single out the contribution from the transverse part to the angular momentum related to the radiation field $\vec{J}_{rad}$ whose components reads:

$$\vec{J}_{rad} = \vec{L} + \vec{S} \tag{1}$$

where $\vec{S}$ is the *spin angular momentum* and $\vec{L}$ represent the *orbital angular momentum* contribution. The spin angular momentum does not depend on the specific coordinate system and hence it is often called as the intrinsic angular momentum. Moreover, since for a massless particle, as a photon, it is not possible to define a rest frame and hence a spin vector, it is possible only to define the projection of the spin along the propagation direction $\hat{z}$, whose values can be $\sigma = \pm s$ with s both integer or half-integer values Enk & Nienhuis (1994). For the photon, having $s = 1$, the helicity σ can takes only values $\sigma = \pm 1$ (in $\hbar$ units). As a form of angular momentum, spin angular momentum is physically associated to the rotation of the particle around its own axis, and for this reason physically is associated to the polarization of single photons. In particular, right-circular polarization is associated to $\sigma = -\hbar$ and left-circular polarization to $\sigma = +\hbar$. On the other hand as shown in eq.(1) light beams carry also orbital angular momentum, considered as the extrinsic component of angular momentum since it depends on the chosen coordinates system. It has been demonstrated that OAM is associated to the azimuthal phase structure of light beams, as will be described in section 3.2 (Allen et al. (1992)). Differently from SAM, OAM causes a rotation of the particle around the beam axis. The experimental evidence of the angular momentum and its components can be achieved only by studying the interaction between light and matter, where it is possible to observe a transfer of angular momentum. In particular, differences between SAM and OAM can be appreciated in the paraxial regime.

3.1 The paraxial approximation

In classical optics a beam that propagates along the $\hat{z}$ direction is described by the Helmoltz equation:

$$\nabla^2 U(\vec{r}) + k^2 U(\vec{r}) = 0 \tag{2}$$

where k is the wavevector $k = \omega c^{-1}$. For beams that are characterized by small divergence angle respect to the propagation direction, eq.(2) can be investigated within the *paraxial approximation*. Such approximation provides a proper description for laser beams, whose beam variation along the transverse plane $(\hat{x}\hat{y})$ are slow compared to the ones along the direction of propagation. In this case the beam can be represented as $U(\vec{r}) = A(\vec{r})e^{-ikz}$, where

the exponential component is the plane wave contribution and $A(\vec{r}) \in \mathbb{C}$ is the complex amplitude whose variations are slow along the beam propagation and thus the following relation holds:

$$\frac{\partial^2 A(\vec{r})}{\partial z^2} << \frac{\partial^2 A(\vec{r})}{\partial^2}, \frac{\partial^2 A(\vec{r})}{\partial y^2} \tag{3}$$

Replacing in eq.(2) the expression of $U(\vec{r})$ and considering the paraxial approximation in eq.(3), we obtain the *paraxial Helmoltz equation*:

$$\frac{\partial^2 A(\vec{r})}{\partial x^2} + \frac{\partial^2 A(\vec{r})}{\partial y^2} - 2ik\frac{\partial A(\vec{r})}{\partial z} = 0 \tag{4}$$

This equation admits different families of solutions depending on the coordinates system adopted. For example adopting Cartesian coordinates, the solutions are the Gaussian beams, widely used in optics to describe laser beams propagation. However if the amplitude $A(\vec{r})$ is modulated by another function slowly varying on direction $\hat{z}$, other valid solutions of eq.(4) can be obtained. Among them, a common one is represented by the Hermite-Gauss (HG) modes, where the Gaussian envelope is multiplied by Hermite polynomials. Interestingly, if instead of a beam described by $U(x, y, z)$ the Helmoltz equation is solved in cylindrical coordinates that is, the function $U(r, \varphi, z)$ is adopted, we obtain another important family of solutions, known as Laguerre-Gauss (LG) modes. As it will be shown in the next section, LG modes are characterized by a dependence of the phase term to the azimuthal angle and hence carry a well-determinate value of orbital angular momentum. Finally, it is worth notice that other classes of solution can be found by adopting polar coordinates (Hypergeometric beams HG Karimi et al. (2007)), or elliptic coordinates (Ince-Gaussian beams), or modifying properly the envelopes (Bessel and Mathieu beams).

3.2 Laguerre-Gauss modes

When the paraxial equation is solved in cylindrical coordinates $(x = rcos\varphi, y = rsin\varphi, z = z)$ the solution is represented by a function family known as Laguerre-Gauss (LG) modes, where the gaussian envelope is multiplied by Laguerre polynomials $L_p^m(\tau)$. The amplitude distribution of these modes reads:

$$u_{p,m}^{LG}(r, \varphi, z) = \frac{C}{\sqrt{1 + \frac{z^2}{z_R^2}}} \left(\frac{r\sqrt{2}}{w(z)}\right)^m L_p^m\left(\frac{2r^2}{w^2(z)}\right) e^{-\frac{r^2}{w^2(z)}} e^{-i\frac{kr^2 z}{2(z^2+z_R^2)}} e^{-im\varphi} e^{i\varsigma(z)} \tag{5}$$

where C is a normalization constant, z_R is the Rayleigh range, $w(z) = w_0\sqrt{1 + \left(\frac{z^2}{z_R^2}\right)}$ is the beam size along $\hat{z}$ starting from the beam waist w_0, and $\varsigma(z) = (2p + m + 1)arctan\frac{z}{z_R}$ is the Gouy phase term. Here (p, m) are the radial and azimuthal index, respectively, and determine the order of the mode $N = 2p + |m|$. In particular (p, m) are integer numbers with $p \geq 0$ while m can assume both positive or negative values. The lowest order of these modes $p = m = 0$ is the Gaussian beam (TEM_{00} mode).

Let us focus on the phase term $e^{-im\varphi}$. This term leads to a phase front that *varies* with the azimuthal angle along the propagation direction: points on the phase front diametrically opposite are indeed dephased by a factor π. This means that the phase front follows an

helicoidal pattern along $\hat{z}$ so that in the center of the transverse plane the contact between all different phases causes a *phase singularity*. The torque shown along the directional axis thus leads to an optical vortex, that is LG beams are characterized by a singularity in the center where the field intensity vanishes. For each optical vortex it is possible to associate a number, known as *topological charge*, that refers to the number of twist over a distance of the wavelength λ. Such number q is always an integer, and can assume both positive or negative values, depending on the direction of the twist. The larger is the number of torsions, greater is the twisting velocity along the beam direction. It is exactly this twisting that leads to a non-vanishing contribution of orbital angular momentum

Fig.(1) reports some examples of LG modes intensities and phases for different values of indices p, m. For $p = 0$ the intensity in the transverse plane is distributed among an annular pattern with a zero-intensity spot in the center, so that LG modes are known also as "doughnut modes". In the next section we will show that Laguerre-Gauss modes constitute a complete orthogonal basis of orbital angular momentum operator L_z eigenvectors, however here we present a notable result of Allen et al. (1992) where for the first time was demonstrated that beam characterized by a helical behavior of the phase front, as for LG modes, carry a well-defined amount of OAM per photon fixed by the value of the azimuthal mode index m

Let us first consider a vector potential written in Cartesian coordinates as:

$$\vec{A}(x,y,z) = u(x,y,z)e^{ikz} \tag{6}$$

Adopting the Lorentz gauge, the relation between magnetic $\vec{B}$ and electric $\vec{E}$ fields and potential vector are known, so that is possible to evaluate the mean value of the Poynting vector $\vec{P}$ that determines the energy carried by the beam:

$$p = \epsilon_0 < \vec{E} \times \vec{B} >= i\omega \frac{\epsilon_0}{2}(u\nabla u^* - u^*\nabla u) + wk\epsilon_0|u|^2$$

This result can be extended to the case of a vector potential expressed in cylindrical coordinates, that is where the beam is characterized by the azimuthal angular dependence $e^{-im\varphi}$. Now we are interested in the estimation of the angular momentum carried by the beam along the $\hat{z}$ direction. The angular momentum reads:

$$\vec{j} = \vec{r} \times \vec{p}$$

where the Poynting vector provides three component $\vec{p} = (p_r, p_\varphi, p_z)$. Thus the component of angular momentum along the propagation direction of the beam j_z can be calculated as $j_z = rp_\varphi$ where:

$$p_\varphi = \epsilon_0 \frac{wm|u|^2}{r} \tag{7}$$

Just by replacing this result in the j_z expression, we get:

$$j_z = \epsilon_0 wm|u|^2 \tag{8}$$

The value of angular momentum carried by each photon can be obtained considering the ratio between angular momentum density and the energy one, and then integrating over all

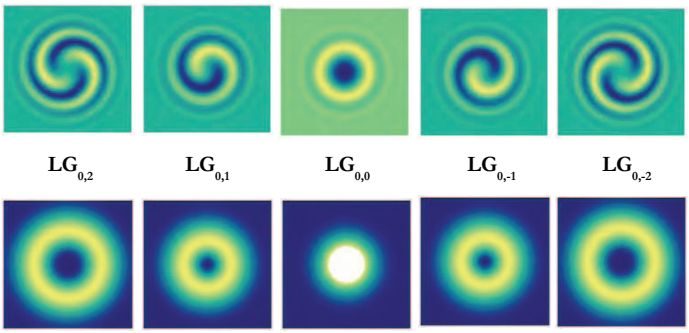

Fig. 1. Examples of LG modes. Top: phase profiles for different LG modes and Bottom: intensity profiles of the same modes.

the transverse plane:

$$\frac{J_z}{W} = \frac{\int\int rdrd\varphi(\vec{r}\times < \vec{E}\times\vec{B} >)_z}{c\int\int rdrd\varphi < \vec{E}\times\vec{B} >_z} = \frac{m}{\omega} \tag{9}$$

Equation (9) shows that each photon that constitutes the beam carries an amount of angular momentum equal to $m\hbar$ Allen et al. (1992; 1999). It is possible to demonstrate that this value refers to the orbital component of angular momentum and is related to the azimuthal phase factor. Indeed if we consider a circularly polarized beam, i.e. a beam with no vanishing contribution of spin angular momentum, its vector potential is:

$$\vec{A} = (\alpha\hat{x} + \beta\hat{y})u(x,y,z)e^{ikz}$$

and going through the same procedure carried before, including the transformation to cylindrical coordinates, the ratio between angular momentum and energy density leads to:

$$\frac{J_z}{W} = \frac{\int\int rdrd\varphi(\vec{r}\times < \vec{E}\times\vec{B} >)_z}{c\int\int rdrd\varphi < \vec{E}\times\vec{B} >_z} = \frac{m}{\omega} + \frac{\sigma}{\omega} \tag{10}$$

We observe from eq.(10) that each photon contributes to the total angular momentum J_z with two components. The σ/ω one belongs to the spinorial contribution, and is due to the polarization of the beam, since $\sigma = \pm 1$ depending on the right or left circular polarization. Analogously, we observe a further term purely related to the phase dependence $e^{-im\varphi}$ that does not belongs to the polarization. Such contribution is thus related to the orbital angular momentum, showing that, depending on the twisting velocity of the phase along the propagation direction, each photon of the beam carries $m\hbar$ OAM.

3.3 Hermite-Gauss modes

The transverse field distribution of laser cavities is typically well described in terms of Hermite-Gauss (HG) modes. These one form a complete orthogonal set that solve the paraxial equation in Cartesian coordinates and their amplitude is given, apart for a phase term, by the product of a gaussian function and Hermite polynomials of indexes $(\tilde{n},\tilde{m})$ Walborn et al.

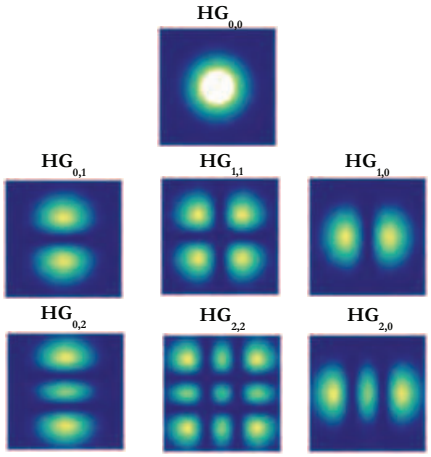

Fig. 2. Intensity profiles for different HG modes. As can be observed, the zero order of HG coincides with the one of LG modes that is, the gaussian mode.

(2005):

$$u^{HG}_{\tilde{n},\tilde{m}} = \sqrt{\frac{2}{2^{(\tilde{n}+\tilde{m})}\pi\tilde{n}!\tilde{m}!}}\frac{1}{w(z)}H_{\tilde{n}}\left(\frac{\sqrt{2}x}{w(z)}\right)H_{\tilde{m}}\left(\frac{\sqrt{2}y}{w(z)}\right)e^{-\frac{x^2+y^2}{w^2(z)}}e^{-ik\frac{(x^2+y^2)z}{2(z^2+z_R^2)}}e^{-i(\tilde{n}+\tilde{m}+1)\varsigma(z)} \quad (11)$$

where $\varsigma(z) = actan\frac{z}{z_r}$ and the last exponential term is the Gouy phase. This solution of the paraxial Helmoltz equation represents modes structurally stables, so that their intensity remain the same along the propagation Allen et al. (1999). The mode indexes $\tilde{n}, \tilde{m}$ define the shape of the beam profile along the $\hat{x}$ and $\hat{y}$ direction, respectively (Saleh & Teich (1991)). Some examples of intensity distribution of such modes are reported in Fig.(2). We observe that the intensity $I_{\tilde{n},\tilde{m}} = |u^{HG}_{\tilde{n},\tilde{m}}|^2$ has $\tilde{n}$ nodes on the horizontal direction, and $\tilde{m}$ along the vertical, while for $\tilde{n} = \tilde{m} = 0$ the shape is the one of a Gaussian beam (TEM_{00} mode). The order of the mode is defined as $N = \tilde{n} + \tilde{m}$. As can be observed from eq.(11), in HG modes each component of the transverse plane travel in phase, as for a plane wave. Indeed this means that surfaces that include all the points with same phase are planes separated by a distance equal to λ. For this reason there is a nil component of linear momentum along the axial direction, which means that such modes do not carry a well defined amount of OAM, as deducible by the lack of the phase term $e^{im\varphi}$. Hermite-Gauss modes form a complete basis set so that any arbitrary field distribution can be written as a superposition of HG modes with indexes $\tilde{n}, \tilde{m}$. However also Laguerre-Gauss modes form a complete basis set, hence a HG mode can be rewritten as a linear superposition of LG modes and *viceversa* through the relations:

$$u^{LG}_{m,p}(x,y,z) = \sum_{k=0}^{N} i^k b(m,p,k) u^{HG}_{N-k,k}(x,y,z) \quad (12)$$

where

$$b(m,p,k) = \frac{(N-k!k!)}{2^N m!p!}^{\frac{1}{2}}\frac{1}{k!}\frac{d^k}{dt^k}[(1-t)^m(1+t)^p]_t = 0 \quad (13)$$

Different indexes that characterize HG and LG are related one set to the other as:

$$m = \tilde{n} - \tilde{m} \tag{14}$$

$$p = min(\tilde{n}, \tilde{m}) \tag{15}$$

Coefficients given in eq.(13) are of crucial importance as they define the matrix element needed for the conversion between HG and LG modes (or viceversa): O'Neil & Courtial (2000). Moreover, the correspondence between HG and LG modes is fixed by the mode order N, defined as:

$$N = \tilde{n} + \tilde{m} = 2p + |m|$$

Inverting relations given in eq.(16) it is possible to estimate the indexes of HG modes in terms of the mode order N and the azimuthal index m:

$$\tilde{n} = \frac{N + m}{2}$$

$$\tilde{m} = \frac{N - m}{2}$$

All these relations can be exploited to generate Laguerre-Gauss modes starting from Hermite-Gauss modes emitted by lasers. Experimentally such mode converters based on eq.(12) are implemented through cylindrical lenses, as explained in section 4.3.

3.4 The orbital angular momentum in quantum mechanics

In 1992 Allen et al. demonstrated that Laguerre-Gauss modes carry a well defined amount of orbital angular momentum through classical mechanics approach, as shown in section 3.2. On the other hand, it is possible to demonstrate this property also following a quantum mechanical approach, showing that LG modes are eigenvectors of the orbital angular momentum operator L_z (Bransden & Joachain (2003); Sakurai (1994)).

The classical orbital angular momentum $\vec{L} = \vec{r} \times \vec{p}$ finds its counterpart in quantum mechanics using the definition of operator momentum $\hat{p} = -i\hbar\nabla$, so that

$$\hat{L} = -i\hbar(r \times \nabla)$$

Thus the cartesian components of the orbital angular momentum operator reads:

$$\begin{aligned} L_x &= -i\hbar \left(y\frac{\partial}{\partial z} - z\frac{\partial}{\partial y} \right) \\ L_y &= -i\hbar \left(z\frac{\partial}{\partial x} - x\frac{\partial}{\partial z} \right) \\ L_z &= -i\hbar \left(x\frac{\partial}{\partial y} - y\frac{\partial}{\partial x} \right) \end{aligned} \tag{16}$$

(17)

where the following commutation rules apply:

$$[L_i, L_j] = i\hbar\epsilon_{ijk}L_k \tag{18}$$

being ϵ_{ijk} the Levi-Civita tensor. It is convenient to study the orbital angular momentum in polar coordinates (r, θ, φ) so that the orbital angular momentum operator L_z can be written as:

$$L_z = -i\hbar \frac{\partial}{\partial \varphi}$$

The eigenvectors equation $L_z \Psi(\varphi) = E\Psi(\varphi)$ with $E = m\hbar$ leads to:

$$\Psi_m(\varphi) = \frac{1}{\sqrt{2\pi}} e^{im\varphi} \tag{19}$$

Moreover the imposition on the eigenvectors to be single valued leads to a constraint on the values of m, that is restricted to positive or negative integers or zero. It emerges from eq.(19) that in paraxial approximation LG modes represent indeed the eigenvectors of the orbital angular momentum operator L_z with eigenvalue $m\hbar$. Generally speaking, any mode with a phase dependence as in eq.(19) can be considered eigenvector of L_z and thus carry a well defined amount of OAM. Laguerre-Gauss modes form a complete Hilbert basis so that can properly represent the quantum photon states in paraxial regime, where spin and orbital contribution can be considered separately. Indeed photon represented by a single LG mode are in a quantum state related to a well-defined value of OAM. It is worth notice that as the eigenvalues of L_z can assume all integer values both positive or negative, the OAM is defined in a infinite-dimensional Hilbert space, thus opening exciting perspectives in the quantum information field.

4. Manipulation of orbital angular momentum

The experimental investigation of orbital angular momentum started in the '90s, thus allowing the idea of OAM as a relatively "'young"' degree of freedom of light. While many devices have been developed for the efficient manipulation of polarization states through birefringent media, as waveplates and polarizing beam splitter, the optical tools for generating and controlling the OAM photon states are rather limited. In last years many efforts have been made in order to implement a device able to generate and manipulate with high efficiency LG modes. In this section we will present the most common and reliable optical devices that exploiting the properties of beams with azimuthal phase structure $e^{im\varphi}$, have allowed the implementation of several quantum optics experiments.

4.1 Computer generated holograms

Computer generated holograms (CGH) are typical tools of diffractive optics, and are probably one of the most common device adopted for the generation and analysis of OAM states. CGHs can be described as diffractive gratings impressed on a film depending on the specific computer-calculated interference pattern formed by a reference plane wave and the desired beam that has to be generated, for example an optical vortex, propagating over a small angle respect to the reference beam. Indeed if a plane wave impinges on the hologram, we would expect to generate on the first diffracted mode an optical vortex equal to the former one. For example, if the reference beam is a LG with OAM m, its interference pattern with a plane wave to be impressed on the hologram is made by a diffraction grating with m lines forming a multi-pronged fork. Depending on the optical vortex that has to be generated/analyzed, a

different hologram is then needed. Each hologram is then characterized by the transmittance function, related to the pattern that has to be impressed on the film. Generally, if we consider as reference optical vortex the beam $E(\varphi,z) = E_0 e^{im\varphi} e^{-ikz}$, and the oblique-propagation plane wave $U(x,z) = e^{i}(k_x x - k_z z)$, the interference pattern at $z = 0$ reads:

$$I = |E(\varphi,z) + U(x,z)|^2 = 1 + I_0 + 2\sqrt{I_0}cos(m\varphi + kx) \tag{20}$$

Taking the Fourier transform of the interference pattern, it is possible to obtain the generic transmittance function for a CGH in polar coordinates:

$$T(r,\varphi) = exp\{i\alpha cos(m\varphi + \frac{2\pi}{\Lambda} r cos\varphi)\} \tag{21}$$

where Λ is the period of the hologram grating, and α the amplitude of phase modulation. In order to illustrate how a hologram actually works, let us consider a standard single-fork hologram ($\Delta m = 1$), characterized by the transmittivity function:

$$T = cos^4\{\frac{1}{2}(\varphi(x,y) + \frac{2\pi}{\Lambda}x)\} \tag{22}$$

where $\varphi(x,y) = arctg\left(\frac{x}{y}\right)$. When a generic wave $E(\rho,\varphi) = E(\rho)e^{im\varphi}$ impinges on the hologram, the output field is determined by $\sqrt{T}E(\rho,\varphi)$, that gives rise to:

$$\frac{E(\rho)}{2}[1 + cos(\varphi(x,y) + \frac{2\pi}{\Lambda}x)]e^{im\varphi} = \frac{E(\rho)}{2}e^{im\varphi} + \frac{E(\rho)}{4}[e^{i(m+1)\varphi}e^{\frac{2\pi}{\Lambda}x} + e^{i(m-1)\varphi}e^{\frac{-2\pi}{\Lambda}x}] \tag{23}$$

Looking at the last term in eq.(23), it emerges how after the hologram the main part of the field is undiffracted and keeps the same value of the initial OAM. On the two first-order diffracted

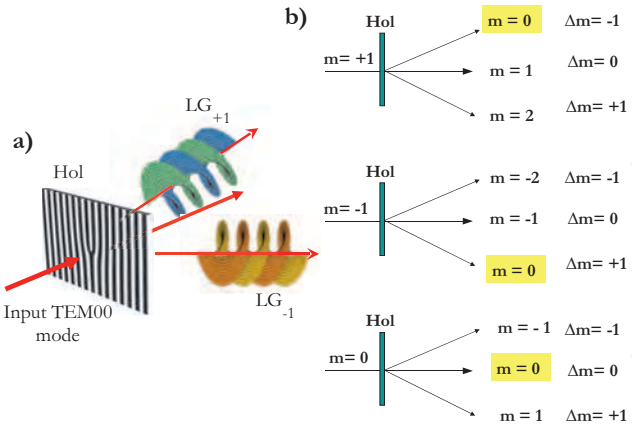

Fig. 3. **a)** Schematic representation of a hologram and its action on an optical field.**b)**Action of a single-fork hologram on different input states. In the yellow box have been enlightened the modes that can be coupled to single mode fiber for analysis.

mode, the beam carries a different value of OAM, equal to $m \pm 1$. A schematic representation of the hologram dynamic is reported in Fig.(3).

Analogously to polarizers, the holograms are used in two ways: (i) for generating a given input quantum state of OAM; (ii) for analyzing a given OAM component of an arbitrary input quantum state. When using the holograms for generating one of the above OAM states, a TEM_{00} input mode is sent into the hologram and the first-order diffracted mode is used for output. The input beam must be precisely centered on the hologram pattern center. When using the holograms for analysis, the input mode, having unknown OAM quantum state, is sent through the hologram (with proper centering). The first-order diffracted output is then coupled to a single-mode fiber, which filters only the $m = 0$ state, before detection. One of the main advantage of holograms device is the possibility to generate and analyze different OAM states, not only LG modes but also their superposition. Unfortunately the efficiency of this device is still low, reaching $\sim 30\%$ for phase holograms (higher transparency), and furthermore any measurement of OAM states in different basis implies a changing of the hologram itself, thus complicating experimental alignment.

4.2 Spiral phase-plates

The spiral phase plate (SPP) principle of function is to directly impose a phase shift on the incident light (Beijersbergen et al. (1994)). They are made by a transparent medium with index of refraction n, whose thickness d gradually varies with the azimuthal angle φ. A schematic representation of such device is reported in Fig.(4). The spiraling increasing thickness let the surface of the SPP look like a single period of helix. As the light beam crosses a dense medium, it is slowed down and hence with the increasing thickness of the plate, there will be a longer optical path corresponding to a wider phase shift δ. In particular each SPP introduces a phase

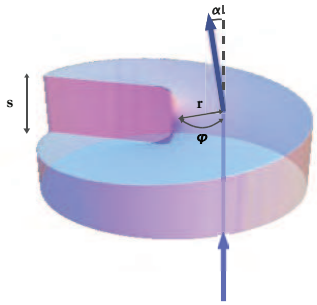

Fig. 4. Schematic representation of a spiral phase plate.

shift δ that is function of the working wavelength λ and of the height of the radial step s:

$$\delta = \frac{(n-1)s}{\lambda}\varphi \tag{24}$$

where we have considered a light beam that travels in the air as surrounding medium of the SPP. The phase shift introduced, due to its dependence to the azimuthal angle, induces a helical structure to the output phase front of the beam that is, a beam carrying orbital angular momentum. In order to design a device able to generate beams with a fixed value of OAM

equal to $m\hbar$, the global phase delay has to be an integer multiple of 2π, which means that the physical height of the step s has to be:

$$s = \frac{m\lambda}{n-1} \tag{25}$$

The main difficulty in the SPP preparation is to properly fix and design the height s. Let us now demonstrate how the SPP generates beams carrying OAM equal to $m\hbar$. A beam is injected on the SPP in a certain position at distance r from the optical axis. The local azimuthal slope of the spiral surface is given by:

$$tan\theta = \frac{s}{2\pi r} \tag{26}$$

Since the beam crosses a dense medium with index of refraction n, it will be deflected by an angle α, determinated by the Snell's law:

$$sin(\alpha + \theta) = nsin\theta \tag{27}$$

For small angles, both the sine as well as the tangent functions can be approximated by the angle itself, hence leading to $\alpha = \theta(n-1)$. After the refraction there will be a non-vanishing component of linear momentum transferred from the SPP in the azimuthal direction, equal to: $p_\varphi \approx \frac{h\alpha}{\lambda}$ Thus the interaction between the SPP and the beam leads to a transfer of a component of orbital angular momentum given by:

$$L_z = rp_\varphi \approx \frac{rh}{\lambda}\alpha = \hbar\frac{s(n-1)}{\lambda} = m\hbar \tag{28}$$

which demonstrates the generation of a beam carrying a well defined value of OAM

Recently *adjustable* spiral phase-plates have been developed, which allow to work for multiple wavelengths in the wavelength region where the material transmits (Rotschild et al. (2004)). In addition, various values of m can be achieved with the same plate by tilting it. They are created by twisting a piece of cracked Plexiglas and orienting the device so that one tab of the phase plate is perpendicular to the incident light. A beam injected at the end of the crack will then produce an optical vortex because of the azimuthally varying tilt around the center of the phase plate.

4.3 Cylindrical lens

Most of the devices usually adopted in quantum optics experiments for the manipulation of OAM states, are not able, in general, to generate pure LG modes, but rather a superposition of modes with same azimuthal mode index. However in order to achieve a pure LG mode it is possible to exploit the relation between LG and HG modes (section 1.1.4) and the possibility to convert one into each other. Such conversion is made possible through the cylindrical lenses: Beijersbergen et al. (1993); Courtial & Padgett (1999).

In section 3.3 we have shown that since both HG and LG modes constitute a complete orthogonal set that solve the paraxial equation, linear superpositions of one set can be used to describe the other (eq.12). A HG mode, whose axes is rotated by 45°, can be expanded into

the same constituent set:

$$u^{HG}_{\tilde{n},\tilde{m}}(\frac{x+y}{\sqrt{2}},\frac{x-y}{\sqrt{2}},z)=\sum_{k=0}^{N} b(n,m,k)u^{HG}_{\tilde{n}+\tilde{m}-k,k}(x,y,z) \tag{29}$$

where all terms are in phase. A device that is able to introduce the phase factor i^k, a phase shift of $\pi/2$ between successive terms in eq.(29), will allow the experimental conversion of HG modes in LG modes. If after implementing this $\frac{\pi}{2}$-converter, a π phase shift is introduced, then it is possible to change the reverse the helicity that is, the OAM sign. In Fig.(5) we report some examples of the transformation between Laguerre-Gauss and Hermite-Gauss modes. It has

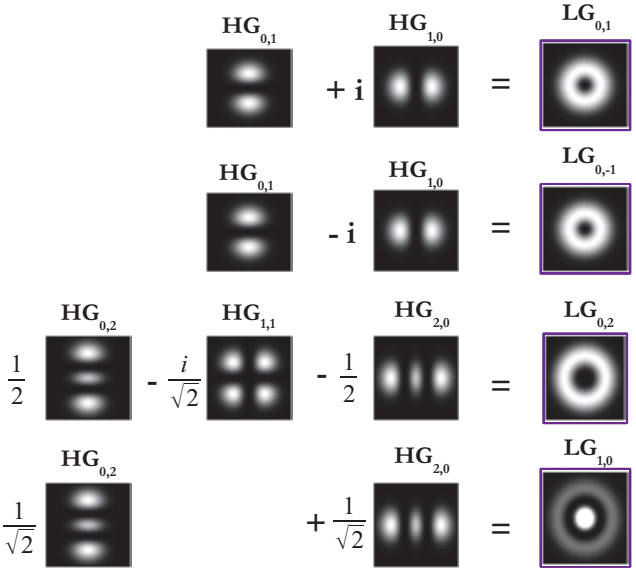

Fig. 5. Examples of transformations between HG and LG modes.

been experimentally demonstrated that a system of cylindrical lenses can implement both the $\frac{\pi}{2}$-converter and the π-converter: Alekseev et al. (1998); Beijersbergen et al. (1993); Courtial & Padgett (1999); Padgett & Allen (2002). Indeed it is possible to exploit the difference in Gouy phase shift between two HG astigmatic modes that take place in a HG mode focused in a cylindrical lens. When we deal with a non-astigmatic beam, the Gouy phase term is expressed by $(\tilde{n}+\tilde{m}+1)\varsigma(z)$. However for astigmatic beams the astigmatism can be characterized in terms of different Rayleigh ranges on planes xz (z_{R_x}) and yz (z_{R_y}), thus leading to a Gouy phase:

$$(\tilde{n}+\frac{1}{2})arctan(\frac{z}{z_{R_x}})+(\tilde{m}+\frac{1}{2})arctan(\frac{z}{z_{R_y}})$$

It has been demonstrated by Beijersbergen et al. (1993) that a system of two identical cylindrical lenses at distance $\pm d$ from the waist of the diagonal HG input beam introduces

a phase difference between two successive terms equal to:

$$\theta = 2[arctan\frac{1}{\beta} - arctan\beta] \quad , \quad \beta = \sqrt{\frac{1-\frac{d}{f}}{1+\frac{d}{f}}} \tag{30}$$

with f focal length of the lenses. The condition $\theta = \pi/2$ is fulfilled for $p = -1 + \sqrt{2}$ that is, for lens with distance $d = f/\sqrt{2}$. The imposition of the mode-matching condition in order to restrict the astigmatism only in the region between the two lenses leads to $z_{R_x} = pd = f - d$ and $z_{R_y} = d/p = f + d$, as Rayleigh range for the input beam. As shown in Fig.(6-**a**), these conditions allow to implement experimentally the $\pi/2$-converter, which can be adopted also as converter from LG to HG modes simply injecting a LG beam and removing the i^k factor. Analogously to the action of a quarter waveplate (QWP) on polarization states, converting linear polarized states in circular polarized ones by introducing a $\pi/2$ phase difference between the linear]y polarized components, the $\pi/2$-converter can be considered as the corresponding device for OAM states, converting a HG to LG by introducing a $\pi/2$ phase difference between the HG components. In order to implement the π-converter, it

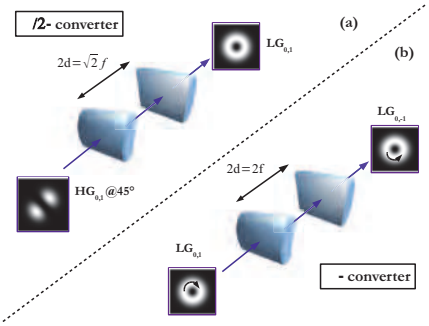

Fig. 6. Schematic representation of **a**: $\pi/2$-converter and **b**: π-converter adopting cylindrical lenses.

is possible to set $\theta = \pi$ which leads to $p = 0$ and thus $d = f$ and a collimated beam ($z_{R_y} \to \infty$). The representation of this converter, that allows to change the sign of m, is reported in Fig.(6-**b**). Once again, a full analogy with a polarization device, the half waveplate (HWP), can be drawn. Indeed the π-converter is similar to the HWP which converts right-circular polarization to left one by introducing a π shift between components.

4.4 Spatial light modulators

The Spatial Light Modulator (SLM) is a device, based on liquid crystals, able to modulate the phase of a light beam or both the intensity and the phase simultaneously (Yoshida et al. (1996)). Besides applications for optical manipulation, SLM are extensively adopted in holographic data storage, and in display technology. A scratch of the SLM structure is reported in Fig.(7). The pure phase SLM adopted for quantum optics experiments are reflective devices in which liquid crystal (LC) is controlled by a direct and accurate voltage, and can modulate a wavefront of light beam (liquid crystal on silicon technology - LCOS). Tha main structure of a SLM is composed by a transparent glass coated with a transparent electrode, then a LC

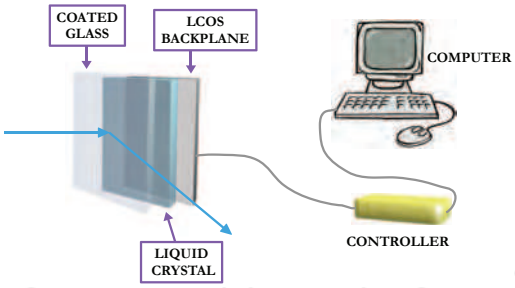

Fig. 7. Schematic representation of a spatial light modulator.

layer and a LCOS backplane, connected to a controller driven by the computer. The LCOS backplane is composed by an array of aluminum pixels, which serve as both reflective mirrors and electrodes. Each electrode is an independently controllable pixel, so that a high-resolution phase modulating array is obtained. Optical modulation is achieved by applying a voltage across the LC layer from the backplane pixels to the transparent electrode on the cover glass. Switching on/off the different pixels composing the backplane, it is then possible to change the refractive index of the LC over them. In this way is possible to create different patterns, like the fork hologram, that can be dynamically modified on demand. The amount of the phase shift depends primarily on three factors: the extraordinary index of the LC material, the thickness of the LC layer, and the wavelength of the input light. As an electric field is applied to a nematic LC layer, there is a corresponding reduction in the extraordinary index of the LC material, and a reduction in the phase shift induced. The main advantage adopting the SLM is then the possibility to work with a dynamic hologram on the same setup. On the other hand, the main disadvantage is the low contrast actually achievable, which is reflected in the efficiency of the device, typically around $10\% - 50\%$.

4.5 The q-plate

When a light beam interacts with matter, a transfer of angular momentum $\vec{J}$ can take place, obeying to the conservation of the global angular momentum of the system. In particular a photon absorbed by a medium can transfer only the spinorial component of angular momentum in *anisotropic* media, while the orbital component can be transferred in *inhomogeneous isotropic* transparent media: Beijersbergen et al. (1993; 1994); Beth (1936). A simultaneous exchange of both spinorial and orbital component of angular momentum is then expected to take place in a medium which is at the same time anisotropic and inhomogeneous. This is precisely the property of liquid crystals. Their structure is determined by the director axis, along witch all the molecules tend to be oriented. By applying electric or magnetic field, or by varying the temperature, it is possible to change the order parameter of the system, and hence change the properties of the LC.

A q-plate (QP) is a birefringent slab having a suitably patterned transverse optical axis, with a topological singularity at its center developed in Naples by Marrucci et al. (2006a). The device is composed by two thin transparent glasses, where in between are inserted some drops of a nematic liquid crystal. The inner surface of the glasses is coated with a polymide for planar alignment, so that it is possible to draw a desired pattern on the glass by simply pressing with

a piece of fabric. Once the q-plate is assembled, the molecules of the LC get oriented following

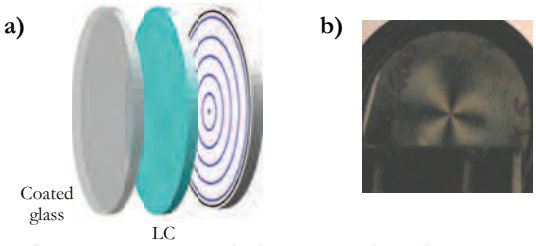

Fig. 8. **a)**Structure of a q-plate device and **b)** Photography of the singularity in a real q-plate device. The picture has been taken by inserting the q-plate between two polaroid films. (Marrucci et al. (2011))

the pattern drawn on the glass. In this way the QP represents an optical device where for each point there is an optical axis in a different position. The specific pattern drawn on the q-plate defines the "charge" q of the singularity that characterize the q-plate. The value of q could be an integer or either a half-integer.

Assuming the normal incidence for the beam of light that crosses the QP, the angle α that defines the local optical axis respect to the singularity of the q-plate is a linear function of the azimuthal angle φ:

$$\alpha(r, \varphi) = q\varphi + \alpha_0 \tag{31}$$

where q is the topological charge, and α_0 a constant. The local direction of the optical axis expressed in eq.(31) enlightens the presence of a topological defect at $r = 0$ that is, at the plane origin.

The working principle of the q-plate is based on the coupling between spin and orbital angular momenta in the NLC in order to exploit an effect similar to the "Pancharatnam-Berry phase" (PBP), already known for the polarization degree of freedom. Such effect is observed when a beam of light undergoes a continuous sequence of transformation on the Poincaré sphere following a closed path. As result, the final wave acquires a phase shift, known as Pancharatnam-Berry phase, that depends on the geometry of the closed path. It has been demonstrated that an analogous effect can be observed in the transverse plane when a wave undergoes a sequence of inhomogeneous polarization transformations having an initial and final homogeneous polarization state. As result, the final beam acquires an inhomogeneous geometrical phase reflected in an overall wave front reshaping, as shown by Marrucci et al. (2006b).

In a single-photon quantum formalism, the QP implements the following quantum transformations on the single photon state:

$$\begin{aligned} |L\rangle_\pi |m\rangle_o &\xrightarrow{QP} |R\rangle_\pi |m+2\rangle_o \\ |R\rangle_\pi |m\rangle_o &\xrightarrow{QP} |L\rangle_\pi |m-2\rangle_o \end{aligned} \tag{32}$$

where $|\cdot\rangle_\pi$ and $|\cdot\rangle_o$ stand for the photon quantum state 'kets' in the polarization and OAM degrees of freedom, and L and R denote the left and right circular polarization states,

respectively. In the following, whenever there is no risk of ambiguity, the subscripts π and o will be omitted for brevity. In Fig.(9) is reported a schematic representation of the QP action. Any coherent superposition of the two input states given in Eq. (32) is expected

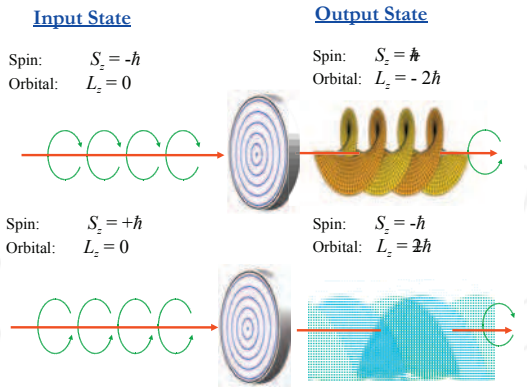

Fig. 9. Schematic representation of the action of a q-plate device with $\delta = \pi$ and $q = 1$, like the ones adopted in our experiments (Marrucci et al. (2011)).

to be preserved by the QP transformation, leading to the equivalent superposition of the corresponding output states, see Nagali et al. (2009). Explicitly, we have

$$\alpha|L\rangle_\pi|m\rangle_o + \beta|R\rangle_\pi|m\rangle_o \xrightarrow{QP} \alpha|R\rangle_\pi|m+2\rangle_o + \beta|L\rangle_\pi|m-2\rangle_o \tag{33}$$

These equations completely define the ideal behavior of the QP on the OAM and polarization subspaces of the photon.

Let us observe that the efficiency of the q-plate device, close to 85%, is related to the birefringent retardation δ introduced by the q-plate itself. An ideal q-plate should have δ uniform across the device and equal to $\delta = \pi$, in order to act on the polarization degree of freedom as a perfect half-waveplate. As have been shown, once a liquid crystal QP is assembled, the birefringent retardation can be tuned either by mechanical compression (exploiting the elasticity of the spacers that fix the thickness of the liquid crystal cell) or by temperature control Karimi et al. (2009), in order to reach the desired value of δ. From eq.(33) it is possible to conclude that for $\delta = \pi$, a QP modifies the OAM state m of a light beam crossing it, imposing a variation $\Delta m = \pm 2q$ whose sign depends on the input polarization, positive for left-circular and negative for right-circular. The handedness of the output circular polarization is also inverted, i.e. the optical spin is flipped (Calvo & Picón (2007)). In the experiments that will be presented in the following, we have adopted only QPs with charge $q = 1$ and $\delta \simeq \pi$. Hence, an input TEM_{00} mode (having $m = 0$) is converted into a beam with $m = \pm 2$.

5. Manipulation of polarization and OAM of single photons

Here we briefly review the experimental results on the adoption of the q-plate device in the single-photon regime.The spin-orbit coupling has been exploited in order to demonstrate the

possibility of adopting the QP as an interface between polarization and OAM of single photon states.

5.1 Single-photon entanglement

The single photon transformations applied by the QP, expressed by eq. (33), describe the coupling of the OAM m and the polarization π degrees of freedom. Interestingly, this property can be exploited to generate single-particle entanglement of π and m degrees of freedom. Indeed when an input photon in a TEM_{00} mode and linear polarization is injected on a q-plate, the output state reads:

$$\left.\begin{array}{l} |H\rangle_\pi |0\rangle_m \\ |V\rangle_\pi |0\rangle_m \end{array}\right\} \stackrel{QP}{\rightarrow} \frac{1}{\sqrt{2}}(|L\rangle_\pi |-2\rangle_m \pm |R\rangle_\pi |+2\rangle_m) \tag{34}$$

This is an entangled state between two qubits encoded in different degrees of freedom. In particular $\{|+2\rangle_m, |-2\rangle_m\}$ is the basis for the OAM qubit which lies in the $|m| = 2$ subspace of the infinite dimensional Hilbert space of orbital angular momentum. The property of the q-plate presented in eq.(34) has been experimentally verified through the reconstruction of the density matrix of the output state emerging from the QP. Such reconstruction is possible by exploiting the quantum state tomography technique (James et al. (2001)), whose peculiarity is to determinate the different elements of the density matrix by analyzing the state in different basis. Hence for the two-qubit quantum state reported in eq.(34), we have performed measurements both in π and m degrees of freedom. Besides the normal $\{|+2\rangle_m, |-2\rangle_m\}$ OAM basis, we had to carry out measurements also in the two superposition bases $\{|a\rangle_m, |d\rangle_m\}$ and $\{|h\rangle_m, |v\rangle_m\}$ by means of different computer-generated holograms Langford et al. (2004). We have considered as incoming states on the QP (**a**) $|H\rangle_\pi |0\rangle_m$,and (**b**) $|V\rangle_\pi |0\rangle_m$. As predicted by the transformation introduced by the QP, when the state $|H\rangle_\pi |0\rangle_m$ is injected, the output state in the basis $\{|L,+2\rangle, |R,-2\rangle\}$ reads:

$$\hat{\rho} = \frac{1}{2}\begin{pmatrix} 0&0&0&0 \\ 0&1&1&0 \\ 0&1&1&0 \\ 0&0&0&0 \end{pmatrix}$$

The experimental reconstruction is reported inf Fig.(10-**a**), with a concurrence of the state equal to $C = (0.95 \pm 0.02)$. Indeed the average experimental concurrence is $C = (0.96 \pm 0.02)$, while the average purity of the states is $P = Tr\rho^2 = (0.94 \pm 0.02)$ (Nagali et al. (2009)).

5.2 Quantum transferrers

Due to its peculiarities, the q-plate provides a convenient way to "interface" the photon OAM with the more easily manipulated spin degree of freedom. Hence as next step we have shown that such interface can be considered as a quantum "transferrer" device, which allows to transfer coherently the quantum information from the polarization π to the OAM m degree of freedom, and *vice versa*. In this Section, we present a complete description of two optical schemes, which have been shown in Nagali et al. (2009), that enable a qubit of quantum information to be transferred from the polarization to the OAM (*transferrer* $\pi \rightarrow o_2$), from OAM to polarization (*transferrer* $o_2 \rightarrow \pi$). Moreover, we tested also the combination of these

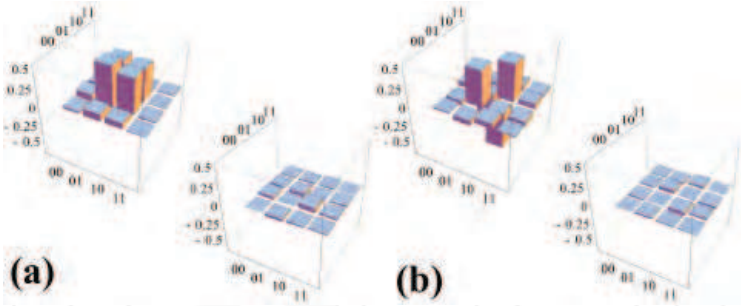

Fig. 10. Experimental density matrices (real and imaginary parts) for the single photon entangled state (Nagali et al. (2009)). The computational values $\{0, 1\}$ are associated to the $\{|R\rangle, |L\rangle\}$ polarization states, and to $\{|+2\rangle, |-2\rangle\}$ for the orbital angular momentum m for the first and the second qubit, respectively. The incoming state on the QP is (**a**) $|H\rangle_\pi|0\rangle_m$,and (**b**) $|V\rangle_\pi|0\rangle_m$.

two schemes, thus realizing the *bidirectional transfer* polarization-OAM-polarization ($\pi \rightarrow o_2 \rightarrow \pi$). The latter demonstration is equivalent to demonstrate quantum communication using OAM for encoding the message. In other words, the qubit is initially prepared in the polarization space, then passed to OAM in a transmitting unit (Alice), sent to a receiving unit (Bob), where it is transferred back to polarization for further processing or detection.

5.2.1 Quantum transferrer $\pi \rightarrow o_2$

Let us consider as initial state the polarization-encoded qubit

$$|\Psi\rangle_{in} = |\varphi\rangle_\pi|0\rangle_o = (\alpha|H\rangle_\pi + \beta|V\rangle_\pi)|0\rangle_o \tag{35}$$

where $|0\rangle_o$ indicates the TEM_{00} mode. By passing it through a pair of suitably oriented quarter-waveplates (one with the optical axis parallel to the horizontal direction and the other at 45°), the photon state is rotated into the L, R basis:

$$(\alpha|L\rangle_\pi + \beta|R\rangle_\pi)|0\rangle_o \tag{36}$$

After the QP the quantum state of the photon is then turned into the following:

$$\alpha|R\rangle|+2\rangle + \beta|L\rangle|-2\rangle. \tag{37}$$

If a polarizer along the horizontal direction is used, we then obtain the state

$$|\Psi\rangle_{out} = |H\rangle_\pi(\alpha|+2\rangle_{o_2} + \beta|-2\rangle_{o_2}) = |H\rangle_\pi|\varphi\rangle_{o_2} \tag{38}$$

which completes the conversion. We note that such conversion process is probabilistic, since the state $|\Psi\rangle_{out}$ is obtained with a probability $p = 50\%$, owing to the final polarizing step. Moreover, since we are using the $\{|H\rangle, |V\rangle\}$ basis for the polarization encoding and the $o_2 = \{|+2\rangle, |-2\rangle\}$ for the OAM one, the transfer is associated also with a rotation of the Poincaré sphere.

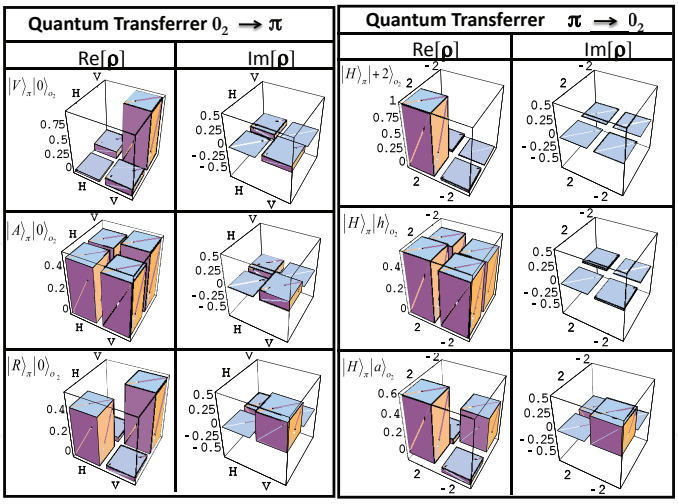

Fig. 11. **Right Side -** Experimental density matrices ρ (the left column shows the real part and right column the imaginary part) measured for the output of the $\pi \rightarrow o_2$ qubit transfer, for each of the three different predicted output states shown in the upper left corner of each row.**Left Side -** Experimental density matrices ρ (the left column shows the real part and right column the imaginary part) measured for the output of the $o_2 \rightarrow \pi$ qubit transfer, for each of the three different predicted output states shown in the upper left corner of each row. (Nagali et al. (2009))

The input arbitrary qubit is written in the polarization using two waveplates, as discussed previously. The experimental results for three specific choices of the input state are shown in Fig. (11). We find a good agreement with theory as demonstrated by the fidelity parameter, with an average fidelity value between the experimental states and the theoretical predictions equal to $F = (97.7 \pm 0.2)\%$.

Thus, we have demonstrated experimentally that the initial information encoded in an input TEM_{00} state can be coherently transferred to the OAM degree of freedom, thanks to the $\pi \rightarrow o_2$ converter, giving rise to the preparation of a qubit in the orbital angular momentum. As the initial information has been stored in the orbital part of the qubit wave-function, new information can be stored in the polarization degree of freedom, allowing the transportation in a single photon of a higher amount, at least two qubits, of information.

5.2.2 Quantum transferrer $o_2 \rightarrow \pi$

Let us now show that the reverse process can be realized as well, by transferring a qubit initially encoded in the OAM subspace o_2 into the polarization space. We therefore consider as initial quantum state of the photon the following one:

$$|\Psi\rangle_{in} = |H\rangle_\pi |\varphi\rangle_{o_2} = |H\rangle(\alpha|+2\rangle + \beta|-2\rangle) \tag{39}$$

By injecting the state $|\Psi\rangle_{in}$ in the q-plate device, and then rotating the output state by means of a pair of waveplates, we obtain the following state:

$$\frac{1}{2}\{\alpha|V\rangle|+4\rangle+\alpha|H\rangle|0\rangle+\beta|V\rangle|0\rangle+\beta|H\rangle|-4\rangle\} \tag{40}$$

Now, by coupling the beam to a single mode fiber, only the states with $m = 0$ that is, the TEM_{00} modes, will be efficiently transmitted. Of course, this implies that a probabilistic process is obtained again, since we discard all the contributions with $m \neq 0$ (ideally, again $p = 50\%$). After the fiber, the output state reads:

$$|\Psi\rangle_{out} = (\alpha|H\rangle + \beta|V\rangle)|0\rangle = |\varphi\rangle_{\pi}|0\rangle_{o} \tag{41}$$

which demonstrates the successful conversion from the OAM degree of freedom to the polarization one. The experimental results for three cases are shown in Fig.(11). We find again a good agreement with theory, with an average fidelity $F = (97.3 \pm 0.2)\%$.

6. Hybrid entanglement

Hybrid entangled states exhibit entanglement between different degrees of freedom of a particle pair. The generation of such states can be useful for asymmetric optical quantum network where the different communication channels adopted for transmitting quantum information exhibit different properties. In such a way one could adopt the suitable degree of freedom with larger robustness along the channel. From a fundamental point of view, the observation of non-locality with hybrid systems proves the fundamental independence of entanglement from the physical realization of the adopted Hilbert space. Very recently the hybrid entanglement of photon pairs between the path (linear momentum) of one photon and the polarization of the other photon has been reported by two different techniques (Ma et al. (2009); Neves et al. (2009)). Nevertheless, the capability of generating hybrid-entangled state encoded in the polarization and OAM of single photons could be advantageous since it could allow the engineering of qubit-qudit entangled states, related to the different Hilbert space dimensionality of the two degrees of freedom. It has been pointed out that such states are desiderable for quantum information and communication protocols, as quantum teleportation, and for the possibility to send quantum information through an optical quantum network composed by optical fiber channels and free-space (Chen & She (2009); Neves et al. (2009)).

In this section we review the realization of hybrid polarization-OAM entangled states, by adopting the deterministic polarization-OAM transferrer described in the previous Section. Polarization entangled photon pairs are created by spontaneous parametric down conversion, the spatial profile of the twin photons is filtered through single mode fibers and finally the polarization is coherently transferred to OAM state for one photon. A complete characterization of the hybrid entangled quantum states has been carried out by adopting the quantum state tomography technique. This result, together with the achieved generation rate, the easiness of alignment and the high quality of the generated state, can make this optical source a powerful tool for advanced quantum information tasks and has been presented in Nagali & Sciarrino (2005).

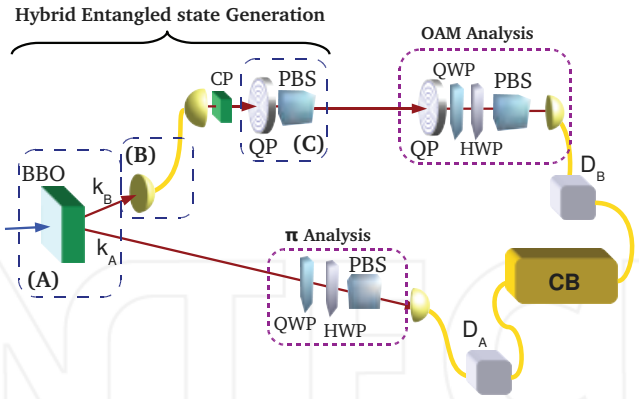

Fig. 12. Experimental setup adopted for the generation and characterization of hybrid π-OAM entangled states (Nagali & Sciarrino (2005)).**(A)** Generation of polarization entangled photons on modes k_A and k_B.**(B)** Projection on the OAM state with $m = 0$ through the coupling on a single mode fiber (SMF).**(C)**Encoding of the state in the OAM subspace o_2 through the $\pi \rightarrow o_2$ transferrer.

6.1 Experimental apparatus and generation of hybrid states

Let us now describe the experimental layout shown in Fig.(12). A 1.5mm thick β-barium borate crystal (BBO) cut for type-II phase matching Kwiat et al. (1995), is pumped by the second harmonic of a Ti:Sa mode-locked laser beam, and generates via spontaneous parametric fluorescence polarization entangled photon pairs on modes k_A and k_B with wavelength $\lambda = 795$ nm, and pulse bandwidth $\Delta\lambda = 4.5$ nm, as determined by two interference filters (IF). The spatial and temporal walk-off is compensated by inserting a $\frac{\lambda}{2}$ waveplate and a 0.75 mm thick BBO crystal on each output mode k_A and k_B Kwiat et al. (1995). Thus the source generates photon pair in the singlet entangled state encoded in the polarization, i.e. $\frac{1}{\sqrt{2}}(|H\rangle^A|V\rangle^B - |V\rangle^A|H\rangle^B)$. The photon generated on mode k_A is sent through a standard polarization analysis setup and then coupled to a single mode fiber connected to the single-photon counter modules (SPCM) D_A. The photon generated on mode k_B is coupled to a single mode fiber, in order to collapse its transverse spatial mode into a pure TEM_{00}, corresponding to OAM $m = 0$. After the fiber output, two waveplates compensate (CP) the polarization rotation introduced by the fiber. To transform the polarization entangled pairs into an hybrid entangled state the photon B is sent through the quantum transferrer $\pi \rightarrow o_2$, which transfers the polarization quantum states in the OAM degree of freedom. After the transferrer operation the polarization entangled state is transformed into the hybrid entangled state:

$$\frac{1}{\sqrt{2}}(|H\rangle_\pi^A|+2\rangle_{o_2}^B - |V\rangle_\pi^A|-2\rangle_{o_2}^B)|0\rangle_o^A|H\rangle_\pi^B \tag{42}$$

In order to analyze with high efficiency the OAM degree of freedom, we exploited the $o_2 \rightarrow \pi$ transferrer. By this approach any measurement on the OAM state is achieved by measuring the polarization after the transferrer device, as shown in Fig.12. Finally the photon has been coupled to a single mode fiber and then detected by D_B connected to the coincidence box (CB), which records the coincidence counts between $[D_A, D_B]$. We observed a final coincidence

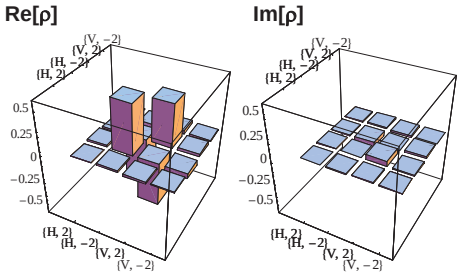

Fig. 13. Experimental density matrix of the hybrid entangled state generated after the transferrer transformation on photons on k_B mode. Each measurement setting lasted 15s (Nagali & Sciarrino (2005)).

rate equal to $C = 100Hz$ within a coincidence window of 3 ns. This experimental data is in agreement with the expected value, determined from $C_{source} = 6kHz$ after taking into account two main loss factors: hybrid state preparation probability p_{prep}, and detection probability p_{det}. p_{prep} depends on the conversion efficiency of the q-plate (0.80 ± 0.05) and on the probabilistic efficiency of the quantum transferrer $\pi \rightarrow o_2$ (0.5), thus leading to $p_{prep} = 0.40 \pm 0.03$. The detection efficiency includes the q-plate conversion efficiency (0.8), the transferrer $o_2 \rightarrow \pi$ (0.5), and the single mode fiber coupling (0.2). Hence $p_{det} = 0.08$.

6.2 Characterization of the state

To completely characterize the state in Eq. (42) we reconstructed the density matrix of the quantum state. The tomography reconstruction requires the estimation of 16 operators James et al. (2001) through 36 separable measurements on the polarization-OAM subspaces. We carried out the reconstruction of the density matrix $\rho^{A,B}_{\pi,o_2}$ after the polarization-OAM conversion. The experimental results are reported in Fig.13, with the elements of the density matrices expressed in the polarization and OAM basis $\{|H,+2\rangle, |H,-2\rangle, |V,+2\rangle, |V,-2\rangle\}$. The fidelity with the singlet states $|\Psi^-\rangle$ has been evaluated to be $F(|\Psi^-\rangle, \rho^{A,B}_{\pi,o_2}) = (0.957 \pm 0.009)$, while the experimental linear entropy of the state reads $S_L = (0.012 \pm 0.002)$. A more quantitative parameter associated to the generated polarization-entangled states is given by the concurrence $C = (0.957 \pm 0.002)$. These values demonstrate the high degree of hybrid entanglement generation.

To further characterize the hybrid quantum states, the violation of Bell's inequalities with the two photon system have been addressed. First, we measured the photon coincidence rate as a function of the orientation of the half-wave plate on Alice arm for two different OAM basis analysis, namely $\{|+2\rangle_{o_2}, |-2\rangle_{o_2}\}$ and $\{|h\rangle_{o_2}, |v\rangle_{o_2}\}$. The variation of the number of coincidences $N(\theta)$ with the angle θ is in agreement with the one expected for entangled states such as $N(\theta) = N_0(1 + cos\theta)$: Fig.14. The coincidence fringe visibility reaches the values $V = (0.966 \pm 0.001)$ and $V = (0.930 \pm 0.007)$. Hence, a non-locality test, the CHSH one (Clauser et al. (1969)), has been carried out. Each of two partners, A (Alice) and B (Bob) measures a dichotomic observable among two possible ones, i.e. Alice randomly measures

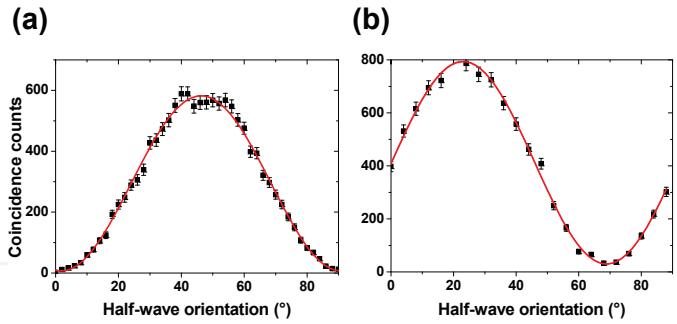

Fig. 14. Coincidence rate $[D_A, D_B]$ measured as a function of the angle θ of the half wave plate on the arm k_A for OAM detected state **(a)** $|+2\rangle$ and **(b)** $|h\rangle_{o_2}$ (Nagali & Sciarrino (2005)).

either **a** or **a'** while Bob measures **b** or **b'**, where the outcomes of each measurement are either $+1$ or -1. For any couple of measured observables $(A = \{\mathbf{a}, \mathbf{a'}\}, B = \{\mathbf{b}, \mathbf{b'}\})$, we define the following correlation function $E(A,B) = \frac{N(+,+)+N(-,-)-N(+,-)-N(-,+)}{N(+,+)+N(-,-)+N(+,-)+N(-,+)}$ where $N(i,j)$ stands for the number of events in which the observables A and B have been found equal to the dichotomic outcomes i and j. Finally we define the parameter S which takes into account the correlations for the different observables

$$S = E(\mathbf{a}, \mathbf{b}) + E(\mathbf{a'}, \mathbf{b}) + E(\mathbf{a}, \mathbf{b'}) - E(\mathbf{a'}, \mathbf{b'}) \tag{43}$$

Assuming a local realistic theory, the relation $|S| \leq S_{CHSH} = 2$ holds. To carry out a non-locality test in the hybrid regime, we define the two sets of dichotomic observables for A and B. For Alice the basis **a** and **a'** correspond, respectively, to the linear polarization basis $\{|H\rangle_\pi, |V\rangle_\pi\}$ and $\{|+\rangle_\pi, |-\rangle_\pi\}$. For Bob the basis **b** and **b'** correspond, respectively, to the OAM basis $\{cos(\frac{\pi}{8})|+2\rangle - sin(\frac{\pi}{8})|-2\rangle, -sin(\frac{\pi}{8})|+2\rangle + cos(\frac{\pi}{8})|-2\rangle\}$ and $\{cos(\frac{\pi}{8})|+2\rangle + sin(\frac{\pi}{8})|-2\rangle, sin(\frac{\pi}{8})|+2\rangle - cos(\frac{\pi}{8})|-2\rangle\}$. Experimentally we obtained the following value by carrying out a measurement with a duration of 60s and an average statistics per setting equal to about 1500 events: $S = (2.51 \pm 0.02)$. Hence a violation by more than 25 standard deviation over the value $S_{CHSH} = 2$ is obtained. This experimental value is in good agreement with an experimental visibility of $V = (0.930 \pm 0.007)$ which should lead to $S = (2.57 \pm 0.02)$.

7. Conclusion

Among all degrees of freedom offered by single photons, the orbital angular momentum (OAM) has a great potential in the quantum information field, as it provides a natural choice for implementing single-photon qudits, the units of quantum information in a higher dimensional space. This can be an important practical advantage, as it enables higher security in quantum cryptographic protocols, as well as implications in fundamental quantum mechanics theory. Moreover, the combined use of different degrees of freedom of a photon, such as OAM and spin, enables the implementation of entirely new quantum tasks.

The authors acknowledge the Future and Emerging Technologies (FET) programme within the Seventh Framework Programme for Research of the European Commission, under FET-Open Grant No. 255914, PHORBITECH.

8. References

Alekseev, A., Alekseev, K., Borodavka, O., Volyar, A. & Fridman, Y. (1998). Conversion of Hermite-Gaussian and Laguerre-Gaussian beams in an astigmatic optical system. 1. Experiment, *Technical Physics Letters* 24(9): 694–696.

Allen, L., Beijersbergen, M. W., Spreeuw, R. J. C. & Woerdman, J. P. (1992). Orbital angular momentum of light and the transformation of laguerre-gaussian laser modes, *Phys. Rev. A* 45(11): 8185–8189.

Allen, L., Padgett, M. & Babiker, M. (1999). The orbital angular momentum of light, *Progress in Optics*, Vol. 39, Elsevier, pp. 291 – 372.
URL: *http://www.sciencedirect.com/science/article/B7W5D-4SFRFMR-8/2/f396ecd62e319c9d81f0234f203b4548*

Andersen, M., Ryu, C., Clade, P., Natarajan, V., Vaziri, A., Helmerson, K. & Phillips, W. (2006). Quantized rotation of atoms from photons with orbital angular momentum, *Phys. Rev. Lett.* 97(17): 170406.

Aolita, L. & Walborn, S. P. (2007). Quantum communication without alignment using multiple-qubit single-photon states, *Phys. Rev. Lett.* 98(10): 100501.

Barreiro, J. T., Langford, N. K., Peters, N. A. & Kwiat, P. G. (2005). Generation of hyperentangled photon pairs, *Phys. Rev. Lett.* 95(26): 260501.

Barreiro, J., Wei, T. & Kwiat, P. (2008). Beating the channel capacity limit for linear photonic superdense coding, *Nature Physics* 4: 282–286.

Beijersbergen, M., Allen, L., Van der Veen, H. & Woerdman, J. (1993). Astigmatic laser mode converters and transfer of orbital angular momentum, *Optics Communications* 96: 123–132.

Beijersbergen, M., Coerwinkel, R., Kristensen, M. & Woerdman, J. (1994). Helical-wavefront laser beams produced with a spiral phaseplate, *Optics Communications* 112(5-6): 321–327.

Beth, R. A. (1936). Mechanical detection and measurement of the angular momentum of light, *Phys. Rev.* 50(2): 115–125.

Bransden, B. & Joachain, C. (2003). *Physics of atoms and molecules*, Pearson Education.

Calvo, G. & Picón, A. (2007). Spin-induced angular momentum switching, *Opt. Lett.* 32(7): 838–840.

Cerf, N. J., Bourennane, M., Karlsson, A. & Gisin, N. (2002). Security of quantum key distribution using *d*-level systems, *Phys. Rev. Lett.* 88(12): 127902.

Chen, L. & She, W. (2009). Increasing Shannon dimensionality by hyperentanglement of spin and fractional orbital angular momentum, *Opt. Lett.* 34(12): 1855–1857.

Clauser, J., Horne, M., Shimony, A. & Holt, R. (1969). Proposed experiment to test local hidden-variable theories, *Phys. Rev. Lett.* 23(15): 880–884.

Courtial, J. & Padgett, M. (1999). Performance of a cylindrical lens mode converter for producing Laguerre-Gaussian laser modes, *Optics Communications* 159(1-3): 13–18.

Enk, S. & Nienhuis, G. (1994). Spin and orbital angular momentum of photons, *EPL (Europhysics Letters)* 25: 497.

Franke-Arnold, S., Allen, L. & Padgett, M. (2008). Advances in optical angular momentum, *Laser & Photonics Reviews* 2(4): 299–313.

Friese, M., Nieminen, T., Heckenberg, N. & Rubinsztein-Dunlop, H. (1998). Optical torque controlled by elliptical polarization, *Optics letters* 23(1): 1–3.

Harke, B., Keller, J., Ullal, C., Westphal, V., Sch
"onle, A. & Hell, S. (2006). Resolution scaling in STED microscopy, *microscopy (STORM)* 3: 793–796.

Hell, S. (2009). Far-field optical nanoscopy, *Single Molecule Spectroscopy in Chemistry, Physics and Biology* pp. 365–398.

James, D. F. V., Kwiat, P. G., Munro, W. J. & White, A. G. (2001). Measurement of qubits, *Phys. Rev. A* 64(5): 052312.

Karimi, E., Piccirillo, B., Nagali, E., Marrucci, L. & Santamato, E. (2009). Efficient generation and sorting of orbital angular momentum eigenmodes of light by thermally tuned q-plates, *Appl. Phys. Lett.* 94(23): 231124.

Karimi, E., Zito, G., Piccirillo, B., Marrucci, L. & Santamato, E. (2007). Hypergeometric-Gaussian modes, *Opt. Lett.* 32(21): 3053–3055.

Kwiat, P. G., Mattle, K., Weinfurter, H., Zeilinger, A., Sergienko, A. V. & Shih, Y. (1995). New high-intensity source of polarization-entangled photon pairs, *Phys. Rev. Lett.* 75(24): 4337–4341.

Langford, N. K., Dalton, R. B., Harvey, M. D., O'Brien, J. L., Pryde, G. J., Gilchrist, A., Bartlett, S. D. & White, A. G. (2004). Measuring entangled qutrits and their use for quantum bit commitment, *Phys. Rev. Lett.* 93(5): 053601.

Lanyon, B. P., Barbieri, M., Almeida, M. P., Jennewein, T., Ralph, T. C., Resch, K. J., Pryde, G. J., O'Brien, J. L., Gilchrist, A. & White, A. G. (2009). Simplifying quantum logic using higher-dimensional hilbert spaces, *Nature Phys.* (7): 134.

Ma, X.-s., Qarry, A., Kofler, J., Jennewein, T. & Zeilinger, A. (2009). Experimental violation of a bell inequality with two different degrees of freedom of entangled particle pairs, *Phys. Rev. A* 79(4): 042101.

Mair, A., Vaziri, A., Weihs, G. & Zeilinger, A. (2001). Entanglement of the orbital angular momentum states of photons, *Nature* 412(6844): 313–316.

Marrucci, L., Manzo, C. & Paparo, D. (2006a). Optical spin-to-orbital angular momentum conversion in inhomogeneous anisotropic media, *Phys. Rev. Lett.* 96(16): 163905.

Marrucci, L., Manzo, C. & Paparo, D. (2006b). Pancharatnam-Berry phase optical elements for wave front shaping in the visible domain: switchable helical mode generation, *Applied Physics Letters* 88: 221102.

Marrucci, L., Karimi, E. Slussarenko, S., Piccirillo, B., Santamato, E., Nagali, E., F. Sciarrino. Spin-to-orbital conversion of the angular momentum of light and its classical and quantum applications, *J. Opt.* 13: 064001 (2011).

Molina-Terriza, G., Rebane, L., Torres, J., Torner, L. & Carrasco, S. (2007). Probing canonical geometrical objects by digital spiral imaging, *J. Europ. Opt. Soc. Rap. Public.* 07014 Vol 2 (2007).

Molina-Terriza, G., Torres, J. & Torner, L. (2007). Twisted photons, *Nature Physics* 3: 305–310.

Nagali, E. & Sciarrino, F. (2005). Generation of hybrid polarization-orbital angular momentum entangled states, *Phys. Rev. Lett* 95: 260501.

Nagali, E., Sciarrino, F., De Martini, F., Marrucci, L., Piccirillo, B., Karimi, E. & Santamato, E. (2009). Quantum information transfer from spin to orbital angular momentum of photons, *Phys. Rev. Lett.* 103: 013601.

Nagali, E., Sciarrino, F., De Martini, F., Piccirillo, B., Karimi, E., Marrucci, L., & Santamato, E. (2009). Polarization control of single photon quantum orbital angular momentum states, *Opt. Expr.* 17:18745.

Neves, L., Lima, G., Delgado, A. & Saavedra, C. (2009). Hybrid photonic entanglement: Realization, characterization, and applications, *Phys. Rev. A* 80(4): 042322.

O'Neil, A. & Courtial, J. (2000). Mode transformations in terms of the constituent Hermite-Gaussian or Laguerre-Gaussian modes and the variable-phase mode converter, *Optics Communications* 181(1-3): 35–45.

Padgett, M. & Allen, L. (2002). Orbital angular momentum exchange in cylindrical-lens mode converters, *Journal of Optics B: Quantum and Semiclassical Optics* 4: S17.

Paterson, C. (2005). Atmospheric turbulence and orbital angular momentum of single photons for optical communication, *Phys. Rev. Lett.* 94(15): 153901.

Poynting, J. H. (1909). The wave motion of a revolving shaft, and a suggestion as to the angular momentum in a beam of circularly polarized light, *Proc. R. Soc. London* 82(557): 560.

Rotschild, C., Zommer, S., Moed, S., Hershcovitz, O. & Lipson, S. (2004). Adjustable spiral phase plate, *Applied optics* 43(12): 2397–2399.

Sakurai, J. (1994). *Modern Quantum Mechanics*, Addison-Wasley.

Saleh, B. E. A. & Teich, M. C. (1991). *Fundamentals of Photonics*, Wiley Interscience.

Shoham, S., O'Connor, D., Sarkisov, D. & Wang, S. (2005). Rapid neurotransmitter uncaging in spatially defined patterns, *Nature Methods* 2(11): 837–843.

Tamburini, F., Anzolin, G., Umbriaco, G., Bianchini, A. & Barbieri, C. (2006). Overcoming the Rayleigh criterion limit with optical vortices, *Phys. Rev. Lett.* 97(16): 163903.

Torner, L., Torres, J. & Carrasco, S. (2005). Digital spiral imaging, *Optics Express* 13(3): 873–881.

Walborn, S. P., Pádua, S. & Monken, C. H. (2005). Conservation and entanglement of hermite-gaussian modes in parametric down-conversion, *Phys. Rev. A* 71(5): 053812.

Yoshida, N., Toyoda, H., Igasaki, Y., Mukohzaka, N., Kobayashi, Y., &Hara, T. (1996). Nonpixellated electrically addressed spatial light modulator (SLM) combining an optically addressed SLM with a CRT, Proc. SPIE 2885: 132-136.

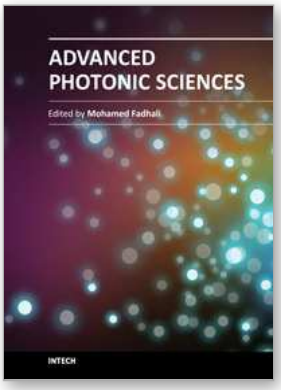

Advanced Photonic Sciences

Edited by Dr. Mohamed Fadhali

ISBN 978-953-51-0153-6
Hard cover, 374 pages
Publisher InTech
Published online 21, March, 2012
Published in print edition March, 2012

The new emerging field of photonics has significantly attracted the interest of many societies, professionals and researchers around the world. The great importance of this field is due to its applicability and possible utilization in almost all scientific and industrial areas. This book presents some advanced research topics in photonics. It consists of 16 chapters organized into three sections: Integrated Photonics, Photonic Materials and Photonic Applications. It can be said that this book is a good contribution for paving the way for further innovations in photonic technology. The chapters have been written and reviewed by well-experienced researchers in their fields. In their contributions they demonstrated the most profound knowledge and expertise for interested individuals in this expanding field. The book will be a good reference for experienced professionals, academics and researchers as well as young researchers only starting their carrier in this field.

INTECH
open science | open minds

InTech Europe
University Campus STeP Ri
Slavka Krautzeka 83/A
51000 Rijeka, Croatia
Phone: +385 (51) 770 447
Fax: +385 (51) 686 166
www.intechopen.com

InTech China
Unit 405, Office Block, Hotel Equatorial Shanghai
No.65, Yan An Road (West), Shanghai, 200040, China
中国上海市延安西路65号上海国际贵都大饭店办公楼405单元
Phone: +86-21-62489820
Fax: +86-21-62489821